GSA Data Repository 2017349

A climatic context for the out-of-Africa migration

Jessica E. Tierney[1], Peter B. deMenocal[2], Paul D. Zander[1]

[1] University of Arizona, Department of Geosciences [2] Lamont-Doherty Earth Observatory of Columbia University

Supplementary Materials and Methods

1. Core site & chronology

Core RC09-166 was collected in 1965 from the *R/V Robert D. Conrad* at 12.15°N, 44.4°E, 738 meters below sea level. The age model for this core was constructed from 11 radiocarbon dates of *Globigerinoides ruber* (white) and 12 tie points between δ^{18}O values of *Globigerinoides ruber* (white) (see below for analytical methods) and the LR04 benthic δ^{18}O stack (*Lisiecki and Raymo*, 2005) (Table S1). We also analyzed benthic δ^{18}O (on *Uvigerina spp.*), and practically speaking the age model would not change substantially if we used the benthic data to establish tiepoints (Figure S1). However, given the location and relatively shallow water depth of our site, benthic δ^{18}O may be substantially influenced by temperature and δ^{18}O of seawater changes associated with Red Sea Overflow water (RSOW) on glacial–interglacial timescales (*Naqvi and Fairbanks*, 1996). This may, for example, explain the unusually enriched values in benthic δ^{18}O observed at the beginning of Marine Isotope Stage 5e (Figure S1). We therefore use tiepoints based on planktonic δ^{18}O. We used the P_Sequence routine in OxCal 4.2 (*Bronk Ramsey*, 1995, 2008) to construct the age model, employing the Marine13 radiocarbon calibration (*Reimer et al.*, 2013) and a reservoir correction (ΔR) of 311$\pm$24 years (1σ) in accordance with our previous chronological work on Gulf of Aden sediment cores (*Tierney et al.*, 2015). The k parameter was set to 0.1. Figure S1 shows the benthic δ^{18}O, planktonic δ^{18}O, and LR04; Figure S2 shows the resulting age model.

2. Oxygen isotope analyses

We conducted δ^{18}O measurements on the planktic foraminifera *Globigerinoides ruber* (white, sensu stricto, 250-350 μm), as well benthic *Uvigerina spp.*. The core was sampled for δ^{18}O measurements every 10 cm. For each sample, approximately 8-10 shells were picked, sonicated in deionized water, and run on an Elementar Isoprime dual inlet stable isotope mass spectrometer with a Multiprep system. Replicate precision of an internal standard over this analysis period was 0.038‰ (1σ) and 0.015‰ (1σ) for δ^{18}O and δ^{13}C, respectively. δ^{18}O results are shown in Figure S1.

3. Organic geochemical analyses

3.1. Sampling and preparation

The core was sampled for organic geochemical analyses every 10 cm. Sediments (already dry) were ground and homogenized, and then extracted using an accelerated solvent extractor (ASE) 350 at a temperature of 100°C and pressure of 1500 psi. The resulting total lipid extracts (TLEs) were evaporated using N_2 gas then purified using column chromatography. TLEs were separated

into five fractions using a 5.75" pipette flash column filled to 1/3 capacity with LC-NH_2 gel and 1/3 capacity with 5% deactivated silica gel. Eluents were hexane (F1), dichloromethane (F2), dichloromethane:isopropanol (2:1) (F3), 4% acetic acid in dichloromethane (F4) and methanol (F5). The fraction containing alkenones (F2) was dried under N_2 gas then redissolved in ethyl acetate for analysis. The fraction containing the fatty acids (F4) was methylated (heated to 50°C, overnight) using acetyl chloride-acidified GC grade methanol of a known isotopic composition. The methylated fatty acids (fatty acid methyl esters; FAMEs) were further purified over 5% deactivated silica gel using hexane and dicholoromethane as respective eluents. The dichloromethane fraction, containing the FAMEs, was dried under N_2 gas and then redissolved in hexane for analysis.

3.2. Analyses

Alkenones

Alkenone $U_{37}^{K'}$ was determined on a Thermo 1310 gas chromatography-flame ionization detector (GC-FID) system equipped with a programmable temperature vaporization (PTV) inlet and a DB-1 column (60 m x 0.32 mm x 0.1 μm). The PTV was operated in splitless mode (splitless time: 3 minutes) with a program of: 60°C (hold 0.1 min) to 325°C at 5°C/sec, and a ramped pressure from 14.5 psi to 33.6 psi. The GC oven program (total runtime: 70 minutes) was: 60°C (hold 2 min) to 270°C at 30°C/min, then to 310°C at 1°C/min (hold 1 min), then to 325°at 10°C/min (hold 18.50 min). Alkenones were detected by comparison of retention times to standards. The $U_{37}^{K'}$ index was calculated as follows:

$$U_{37}^{K'} = \frac{\text{C37:2}}{\text{C37:3} + \text{C37:2}} \tag{1}$$

where C37:2 and C37:3 are the peak areas of the di- and tri- unsaturated C_{37} alkenones. The precision of the alkenone determination was 0.002 $U_{37}^{K'}$ units based on repeat measurements of a laboratory sediment standard. To convert $U_{37}^{K'}$ to SSTs, we used the Indian Ocean calibration of (*Sonzogni et al.*, 1997):

$$U_{37}^{K'} = 0.023 \cdot SST + 0.316 \tag{2}$$

The (*Sonzogni et al.*, 1997) calibration has a smaller slope (0.023) than the global calibrations (0.033) to account for the reduced sensitivity of $U_{37}^{K'}$ to SST changes at warm SST. The maximum possible temperature using this calibration (the point at which $U_{37}^{K'}$=1) is 29.7°C. The data from RC09-166 generally stay well below this limit and only exceed 29°C during MIS 5e and MIS 7 (Figure 2). As noted in the main text, RC09-166 $U_{37}^{K'}$ shows close agreement with core MD90-963. It also agrees well with two cores from the Arabian Sea upwelling zone, TY92-929/P and ODP 723A (*Rostek et al.*, 1997), which sit within much cooler waters (mean annual SSTs of ca. 24°C) but still show a warm MIS 6. This confirms that the lack of glacial-interglacial

variability between MIS 7–5 at RC09-166 is not due to saturation of the proxy.

Leaf wax isotopes

The hydrogen and carbon isotopic compositions of the FAMEs were measured via gas chromatography-isotope ratio monitoring mass spectrometry using a Thermo Finnigan Delta V Plus mass spectrometer. H_2 and CO_2 gases calibrated to an authentic *n*-alkane standard (the "A6" mix, provided by Arndt Schimmelmann at Indiana University) were used as references for each analysis. In addition, a synthetic mix of FAMEs was analyzed every 10 samples to monitor drift and correct for any offsets. Samples were run at least in duplicate. The precision of repeat analyses was 2‰ for δD and 0.2‰ for δ^{13}C. We applied mass balance corrections for the addition of the methyl group during the methylation process, where δD_{meoh} was determined to be -83±1‰ and $\delta^{13}C_{meoh}$ was determined to be -42.7±0.5‰ by repeat measurements of a phthalic acid standard of a known isotopic composition (provided by Arndt Schimmelmann at Indiana University) methylated with the same methanol used for the methylation of the target compounds. We measured the C_{30} fatty acid as the representative terrestrial leaf wax (hereafter, δD_{wax}) due to evidence that fatty acids of shorter chain lengths could have a competing aquatic origin in the marine environment (*Kusch et al.*, 2010). This is the same chain length that we previously analyzed in nearby core P178-15P (*Tierney and deMenocal*, 2013).

To isolate the hydroclimatic component of the δD_{wax} signal, we correct the δD_{wax} data for ice volume effects by assuming a Last Glacial Maximum change in global δ^{18}O of seawater of 1‰ (*Schrag et al.*, 1996) and scaling the benthic oxygen isotope stack (*Lisiecki and Raymo*, 2005) – a proxy for the changes in global ice volume – accordingly. We then removed the ice volume change from the data using the following equation:

$$\delta D_{wax-corr} = \frac{1000 + \delta D_{wax}}{8 \times 0.001 \times \delta^{18}O_{ice} + 1} - 1000 \quad (3)$$

Figure S3 shows the both the corrected and uncorrected δD_{wax} as well as $\delta^{13}C_{wax}$ data. Studies assessing the isotopic fractionation ($\varepsilon_{water-wax}$) between δD_{wax} and precipitation δD (δD_P) indicate that $\varepsilon_{water-wax}$ differs by plant growth form; thus, changing landscapes through time may affect mean $\varepsilon_{water-wax}$ and therefore δD_{wax} (*Sachse et al.*, 2012). The most significant difference appears to be between monocots (grasses) and dicots (*Gao et al.*, 2014). In East Africa, grasses are primarily C_4 grasses, so $\delta^{13}C_{wax}$ can be used to track C_4 grass contributions through time and if necessary, correct δD_{wax} for large shifts (*Magill et al.*, 2013; *Feakins*, 2013). In this case, $\delta^{13}C_{wax}$ varies by 3‰ or less over the last 200 ka and is not significantly correlated with δD_{wax} ($r = -0.19, p = 0.56$), indicating that the contribution of C_4 plants to C_{30} leaf wax was relatively stable through time (Fig. S2). We therefore do not adjust δD_{wax} for changing vegetation type.

Given the large shifts in δD_{wax}, it may seem unusual that $\delta^{13}C_{wax}$ is relatively constant. However, while $\delta^{13}C_{wax}$ has been used as a proxy for aridity elsewhere in Africa, in arid environments such as the Horn of Africa and the Sahara previous leaf wax δD_{wax} and $\delta^{13}C_{wax}$ studies demonstrate that it commonly does not follow δD_{wax} and has a complex signature (*Tierney and deMenocal*, 2013; *Feakins*, 2013; *Liddy et al.*, 2016; *Tierney et al.*, 2017). This is likely due to the nature of landscapes in arid to semiarid regions, which does not linearly translate to changes in C_4 vegetation. At the lowest rainfall rates, the landscape is dominated by C_3 shrubs; at moderate rainfall rates, C_4 grasslands dominate; and when rainfall increases further, then a C_3-C_4 mixed savanna/dry forest emerges (*Feakins*, 2013). Thus, a decrease in $\delta^{13}C_{wax}$ could indicate either an increase or decrease in rainfall and coeval behavior with δD_{wax} is not expected. δD_{wax} remains the best indicator for aridity in locations like the Horn of Africa, and it is validated by the clear decrease during the early Holocene African Humid Period, when paleolake shorelines indicate high lake levels throughout North and East Africa as well as the Arabian peninsula (*deMenocal and Tierney*, 2012).

References

Atkinson, Q. D., R. D. Gray, and A. J. Drummond (2009), Bayesian coalescent inference of major human mitochondrial DNA haplogroup expansions in Africa, *Proceedings of the Royal Society of London B: Biological Sciences*, *276*(1655), 367–373.

Bowler, J. M., H. Johnston, J. M. Olley, J. R. Prescott, R. G. Roberts, W. Shawcross, and N. A. Spooner (2003), New ages for human occupation and climatic change at Lake Mungo, Australia, *Nature*, *421*(6925), 837–840.

Bronk Ramsey, C. (1995), Radiocarbon calibration and analysis of stratigraphy: the OxCal program, *Radiocarbon*, *37*(2), 425–430.

Bronk Ramsey, C. (2008), Deposition models for chronological records, *Quaternary Science Reviews*, *27*(1), 42–60.

deMenocal, P., and J. Tierney (2012), Green Sahara: African humid periods paced by Earth's orbital changes, *Nature Education Knowledge*, *3*(10), 12.

Feakins, S. J. (2013), Pollen-corrected leaf wax D/H reconstructions of northeast African hydrological changes during the late Miocene, *Palaeogeography, Palaeoclimatology, Palaeoecology*, *374*, 62–71.

Fu, Q., A. Mittnik, P. L. Johnson, K. Bos, M. Lari, R. Bollongino, C. Sun, L. Giemsch, R. Schmitz, J. Burger, et al. (2013), A revised timescale for human evolution based on ancient mitochondrial genomes, *Current Biology*, *23*(7), 553–559.

Gao, L., E. J. Edwards, Y. Zeng, and Y. Huang (2014), Major evolutionary trends in hydrogen isotope fractionation of vascular plant leaf waxes, *PloS One*, *9*(11), e112610.

Karmin, M., L. Saag, M. Vicente, M. A. W. Sayres, M. Järve, U. G. Talas, S. Rootsi, A.-M. Ilumäe, R. Mägi, M. Mitt, et al. (2015), A recent bottleneck of Y chromosome diversity coincides with a global change in culture, *Genome Research*, *25*(4), 459–466.

Kusch, S., J. Rethemeyer, E. Schefuß, and G. Mollenhauer (2010), Controls on the age of vascular plant biomarkers in Black Sea sediments, *Geochimica et Cosmochimica Acta*, *74*(24), 7031–7047.

Liddy, H. M., S. J. Feakins, and J. E. Tierney (2016), Cooling and drying in northeast Africa across the Pliocene, *Earth and Planetary Science Letters*, *449*, 430–438.

Lisiecki, L. E., and M. E. Raymo (2005), A Pliocene-Pleistocene stack of 57 globally distributed benthic delta O-18 records, *Paleoceanography*, *20*(1), PA1003, doi:10.1029/2004PA001071.

Magill, C. R., G. M. Ashley, and K. H. Freeman (2013), Water, plants, and early human habitats in eastern Africa, *Proceedings of the National Academy of Sciences*, *110*(4), 1175–1180.

Malaspinas, A.-S., M. C. Westaway, C. Muller, V. C. Sousa, O. Lao, I. Alves, A. Bergström, G. Athanasiadis, J. Y. Cheng, J. E. Crawford, et al. (2016), A genomic history of Aboriginal Australia, *Nature*, *538*, 207–214.

Naqvi, W. A., and R. G. Fairbanks (1996), A 27,000 year record of Red Sea outflow: Implication for timing of post-glacial monsoon intensification, *Geophysical Research Letters*, *23*(12), 1501–1504.

Posth, C., G. Renaud, A. Mittnik, D. G. Drucker, H. Rougier, C. Cupillard, F. Valentin, C. Thevenet, A. Furtwängler, C. Wißing, et al. (2016), Pleistocene mitochondrial genomes suggest a single major dispersal of Non-Africans and a Late Glacial population turnover in Europe, *Current Biology*, *26*(6), 827–833.

Reimer, P. J., E. Bard, A. Bayliss, J. W. Beck, P. G. Blackwell, C. B. Ramsey, C. E. Buck, H. Cheng, R. L. Edwards, M. Friedrich, et al. (2013), IntCal13 and Marine13 radiocarbon age calibration curves 0–50,000 years cal BP, *Radiocarbon*, *55*(4), 1869–1887.

Rieux, A., A. Eriksson, M. Li, B. Sobkowiak, L. A. Weinert, V. Warmuth, A. Ruiz-Linares, A. Manica, and F. Balloux (2014), Improved calibration of the human mitochondrial clock using ancient genomes, *Molecular Biology and Evolution*, *31*(10), 2780–2792.

Rostek, F., E. Bard, L. Beaufort, C. Sonzogni, and G. Ganssen (1997), Sea surface temperature and productivity records for the past 240 kyr in the Arabian Sea, *Deep Sea Research Part II: Topical Studies in Oceanography*, *44*(6), 1461–1480.

Sachse, D., I. Billault, G. J. Bowen, Y. Chikaraishi, T. E. Dawson, S. J. Feakins, K. H. Freeman, C. R. Magill, F. A. McInerney, M. T. J. van der Meer, P. Polissar, R. J. Robins, J. P. Sachs, H.-L. Schmidt, A. L. Sessions, J. W. C. White, J. B. West, and A. Kahmen (2012), Molecular paleohydrology: interpreting the hydrogen-isotopic composition of lipid biomarkers from photosynthesizing organisms, *Annual Reviews of Earth and Planetary Science*, *40*, 221–249.

Sankararaman, S., N. Patterson, H. Li, S. Pääbo, and D. Reich (2012), The date of interbreeding between Neandertals and modern humans, *PLoS Genetics*, *8*(10), e1002,947.

Schrag, D. P., G. Hampt, and D. W. Murray (1996), Pore fluid constraints on the temperature and oxygen isotopic composition of the glacial ocean, *Science*, *272*, 1930–1932.

Sonzogni, C., E. Bard, F. Rostek, D. Dollfus, A. Rosell-Melé, and G. Eglinton (1997), Temperature and salinity effects on alkenone ratios measured in surface sediments from the Indian Ocean, *Quaternary Research*, *47*(3), 344–355.

Tierney, J. E., and P. B. deMenocal (2013), Abrupt Shifts in Horn of Africa Hydroclimate Since the Last Glacial Maximum, *Science*, *342*, 843–846.

Tierney, J. E., C. C. Ummenhofer, and P. B. deMenocal (2015), Past and future rainfall in the Horn of Africa, *Science Advances*, *1*(9), e1500682.

Tierney, J. E., F. S. Pausata, et al. (2017), Rainfall regimes of the Green Sahara, *Science Advances*, *3*(1), e1601503.

Table S1. Radiocarbon dates and tie points used to construct the age model for core RC09-166. Radiocarbon measurements were made at the Woods Hole Oceanographic Institution National Ocean Sciences Accelerator Mass Spectrometry (NOSAMS) lab.

Accession #	Depth (cm)	^{14}C/tiepoint Age	Error (1σ)	OxCal Age (BP)	Error (1σ)
		— ^{14}C dates —			
OS-121824	5.5	2570	15	1884	44
OS-121825	25.5	2970	15	2359	44
OS-121826	55.5	5280	20	5333	50
OS-121827	75.5	7230	25	7443	37
OS-121828	95.5	8810	35	9143	71
OS-121829	125.5	12250	40	13402	59
OS-121830	165.5	17500	75	20271	122
OS-121833	185.5	23000	140	26452	196
OS-121831	215.5	23700	160	27371	140
OS-121832	255.5	33000	500	36201	625
OS-121834	305.5	39200	1100	42933	942
		— Tiepoints —			
N/A	335.5	55000	2000	53922	1740
N/A	375.5	62000	2000	61085	1643
N/A	445.5	69000	2000	70264	1724
N/A	515.5	87000	2000	86669	1853
N/A	625.5	109000	2000	108847	1862
N/A	765.5	135000	2000	135335	1856
N/A	845.5	154000	2000	152669	1817
N/A	1026.5	174000	2000	175877	1853
N/A	1065.5	188000	2000	186873	1623
N/A	1095.5	192000	2000	191272	1537
N/A	1166.5	200000	2000	199925	1547
N/A	1215.5	205000	2000	205669	1691

Table S2. List of published genetic and fossil dates (plotted in Fig. 3) used to constrain the primary out-of-Africa event from 55–65 ka.

Haplogroup/Event	Age	95% CI	Reference
L3 (mtDNA)	73.5	61–86	(*Atkinson et al.*, 2009)
L3 (mtDNA)	78.3	62.4–94.9	(*Fu et al.*, 2013)
L3 (mtDNA)	72	54–93	(*Rieux et al.*, 2014)
CT (YDNA)	69.0	53.8–85.8	(*Karmin et al.*, 2015)
M (mtDNA)	48.8	43.6–54.8	(*Posth et al.*, 2016)
N (mtDNA)	50.3	46.9–55.1	(*Posth et al.*, 2016)
C (YDNA)	50.9	38.3–61.9	(*Karmin et al.*, 2015)
D (YDNA)	49.9	37.0–61.7	(*Karmin et al.*, 2015)
Aboriginal Australian divergence	57.9	51.1–72.1	(*Malaspinas et al.*, 2016)
AMH–Neanderthal admixture	56	47 – 65	(*Sankararaman et al.*, 2012)
AMH fossils in Australia	48	46 – 50	(*Bowler et al.*, 2003)

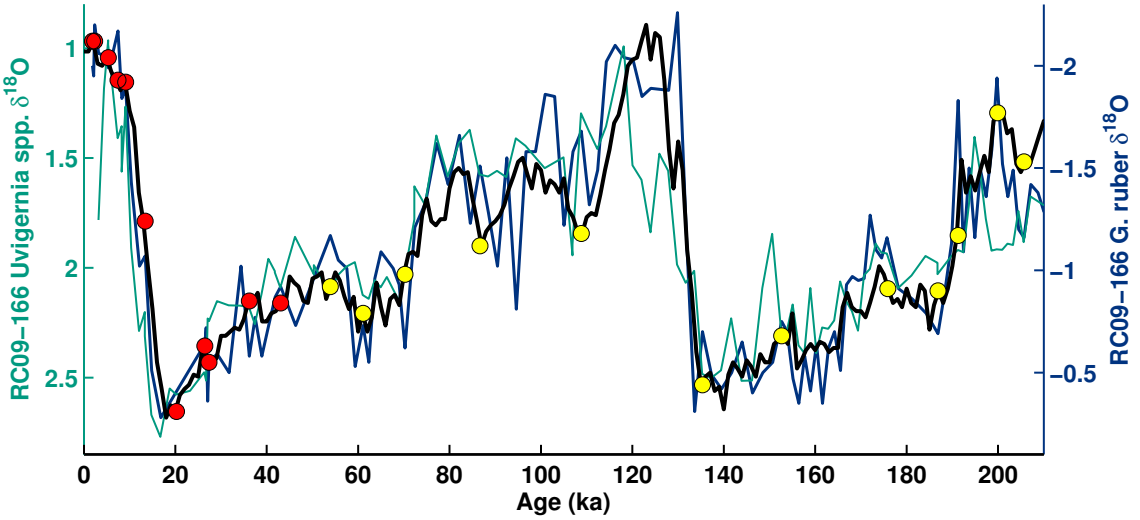

Figure S1. δ^{18}O measurements of benthic *Uvigerina spp.* (in teal), planktonic *G. ruber* (in blue) from core RC09-166 compared to the benthic stack (LR04, in black). Radiocarbon dates are plotted in red, tiepoints between the *G. ruber* δ^{18}O data and benthic stack are plotted in yellow.

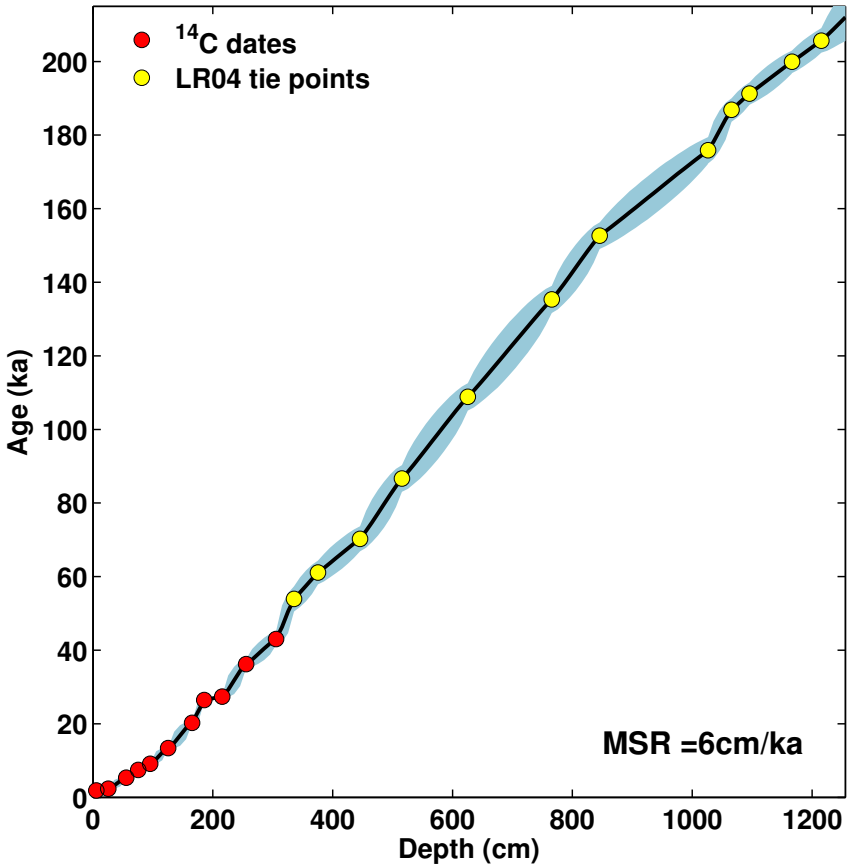

Figure S2. Age model for core RC09-166. ^{14}C-dated intervals are plotted in red, tiepoints between the *G. ruber* δ^{18}O data and benthic δ^{18}O stack (LR04) are plotted in yellow, and the median age model is plotted in black. Lighter blue error bars denote 2σ uncertainties. Mean sedimentation rate (MSR) is displayed in the corner of the plot.

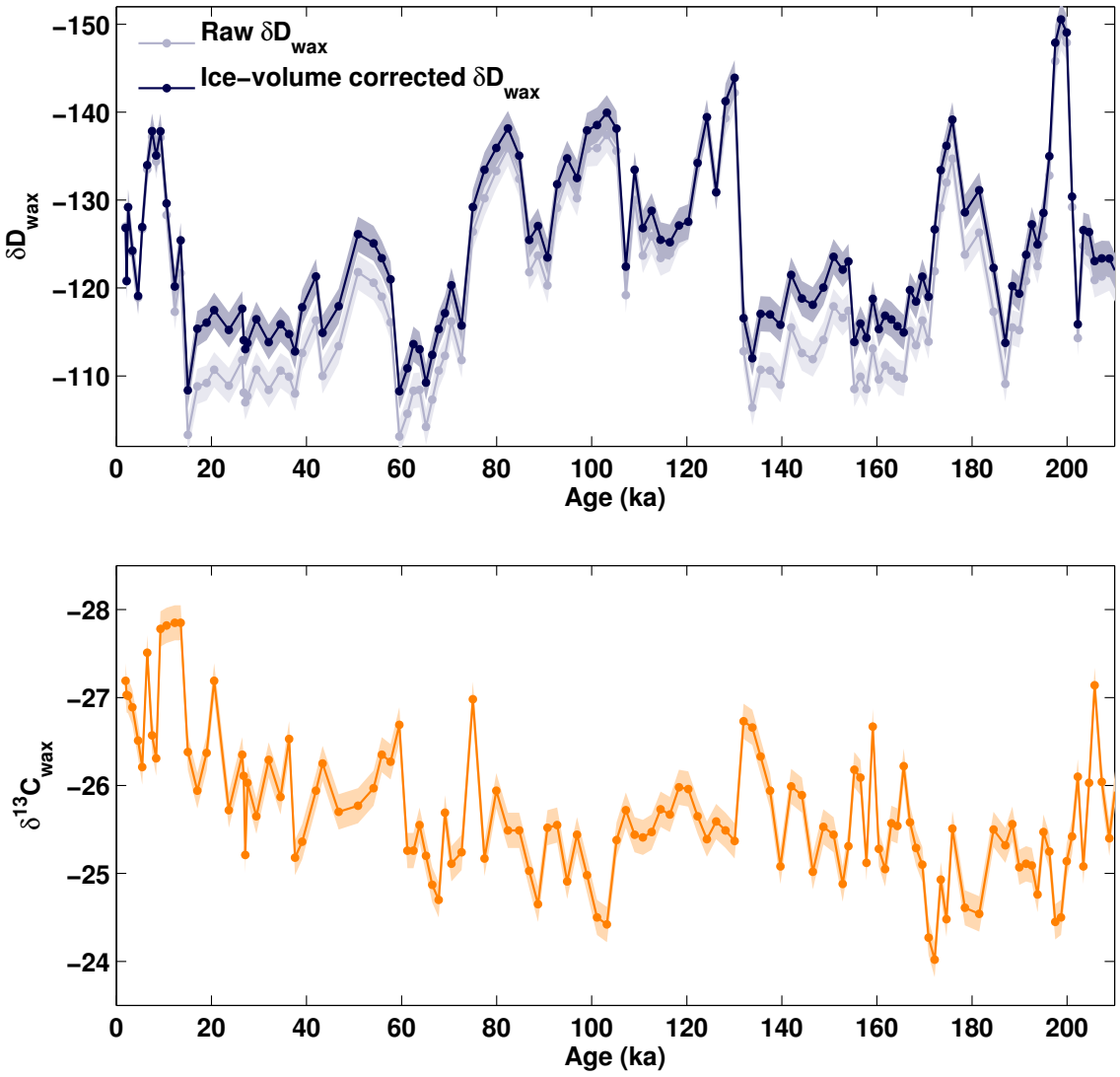

Figure S3. At top, $\delta\mathrm{D}_{wax}$ data, raw and corrected for ice volume contributions. At bottom, $\delta^{13}\mathrm{C}_{wax}$ data. Data are plotted with analytical 1σ error bars.